recommended

e guide

The Fundamentals of Neutron Powder Diffraction

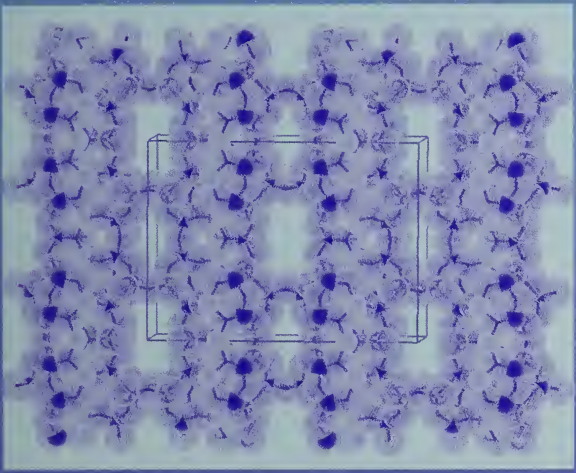

John R.D. Copley

NIST
National Institute of Standards and Technology
Technology Administration
U.S. Department of Commerce

Special
Publication
960-2

NIST Recommended Practice Guide

Special Publication 960-2

The Fundamentals of Neutron Powder Diffraction

John R.D. Copley

Materials Science and
Engineering Laboratory

November 2001

U.S. Department of Commerce
Donald L. Evans, Secretary
Technology Administration
Phillip J. Bond, Under Secretary for Technology
National Institute of Standards and Technology
Karen H. Brown, Acting Director

National Institute of Standards and Technology
Special Publication 960-2
Natl. Inst. Stand. Technol.
Spec. Publ. 960-2
40 pages (November 2001)
CODEN: NSPUE2
U.S. GOVERNMENT PRINTING OFFICE
WASHINGTON: 2001

For sale by the Superintendent of Documents
U.S. Government Printing Office
Internet: bookstore.gpo.gov Phone: (202) 512-1800 Fax: (202) 512-2250
Mail: Stop SSOP, Washington, DC 20402-0001

I. INTRODUCTION

I.1. Structure and Properties

Information about the organization of the atoms in materials is essential to any attempt at a detailed understanding of their physical, chemical and mechanical properties. Richard Feynman put it this way (Feynman et al., 1963): "If they will tell us, more or less, what the earth or the stars are like, then we can figure it out. In order for physical theory to be of any use, we must know where the atoms are located." Consider the example of diamond and graphite. Diamond is one of the hardest materials known whereas graphite is so soft that it is used in pencils and as a lubricant, yet both materials are pure carbon. The reason for this dramatic difference is that the atoms are arranged very differently. In diamond they assemble into a rigid three-dimensional network but in graphite they are arranged in parallel sheets and a small force is sufficient to cause the sheets to slip. Examples abound in other fields such as protein chemistry, where "the understanding of mechanism is based on knowing the structures and properties of the reagents and the kinetics and thermodynamics of their reactions, as well as how the kinetics and other properties change when the structures of the reagents are modified and the reaction conditions are altered." (Fersht, 1999)

I.2. Diffraction

The most widely used (and the most powerful) method of studying atomic structure is known as diffraction. Electrons are used to examine structure in thin sections of material or close to a material surface, whereas x-rays and neutrons are the probes of choice for looking at the bulk. X-rays are normally used because laboratory instruments are readily available from various manufacturers. Furthermore high brilliance sources, such as the Advanced Photon Source at Argonne National Laboratory, may be used when intensity is a problem. Despite the widespread use of x-rays there are situations where thermal neutrons are the better choice, as well as situations where the combined use of x-rays and neutrons is beneficial. In sections II.5 and II.6 we shall compare and contrast x-rays and neutrons.

I.3. The Meaning of "Structure"

The positions of the atoms in a material define its atomic structure. In a gas or liquid the atoms move throughout the available volume, and the structure is described using one or more "pair distribution functions" which are probability distributions of instantaneous distances between pairs of atoms. The atoms in a solid behave quite differently, for the most part moving back and forth about their equilibrium positions, and pair distribution functions can again be used to describe the structure. The pair distribution approach is most useful when applied to non-crystalline solids such as glasses, in which the mean (time-averaged) positions of the atoms lack long range order. In crystalline solids the mean positions of the atoms have a regularity that persists over large distances in all directions, and the structure is specified by the mean positions of the atoms (together with information that describes site occupancies and mean displacement amplitudes).

I.4. Crystals and Powders

Crystalline solids may be classified according to how the individual crystallites within the material are organized. At one extreme is the single crystal, which consists of one or more crystallites with virtually the same orientation. At the other extreme is the polycrystalline sample in which all possible orientations of crystallites are presumed to be equally likely. A third possibility is the intermediate case of a polycrystalline sample in which the distribution of crystallite orientations is neither uniform nor strongly peaked. This latter type of sample is often described as a sample with preferred orientation or "texture," and an important sub-field of applied neutron diffraction is the study of texture (Prask and Choi, 1993, and references therein). In what follows we shall be concerned with experiments on "powders," i.e., polycrystalline samples which are presumed to have a uniform distribution of orientations.

I.5. Scattering, Diffraction and Absorption

When a beam of neutrons strikes a material several things can happen. Some will be absorbed, others will emerge in a new direction with or without a change in energy, and the rest will pass through the material unaffected. Those that emerge in a new direction are described as "scattered" neutrons, and the investigation of materials by measuring how they scatter neutrons is known as neutron scattering. Neutron "diffraction," as opposed to "scattering," generally implies that there is no attempt to determine the neutron's change in energy when it is scattered. Neutron diffraction (Bacon 1975) is a powerful and popular technique, which is primarily used to determine the structures of crystalline materials. It is also used to determine magnetic structures and to study pair distribution functions in non-crystalline solids, liquids and gases.

II. METHODS

II.1. Definitions

A low energy (non-relativistic) neutron has energy E, wave vector **k**, velocity v, and wavelength λ. These quantities are related as follows:

$$|\mathbf{k}| = \frac{2\pi}{\lambda}; \quad \lambda = \frac{h}{mv}; \quad E = \frac{1}{2}mv^2 = \frac{h^2}{2m\lambda^2}, \qquad (1)$$

where h is Planck's constant and m is the mass of the neutron. Approximate conversions are as follows:

$$E[\text{meV}] \approx \frac{82}{(\lambda[\text{Å}])^2}, \quad v[\text{mm}/\mu\text{s}] \approx \frac{4}{\lambda[\text{Å}]}.$$

The most commonly used units of neutron wavelength and energy are the Ångström (Å) and the milli-electron volt (meV) respectively. Note that 1 Å=0.1 nm and 1 meV ≈ 8.1 cm^{-1} ≈ 11.6 K ≈ 0.24×10^{12} Hz ≈ 1.6×10^{-15} erg. Hence 1 kJ/mol ≈ 10.4 meV/molecule. Much more exact conversion factors can be derived using the recommended values of the fundamental physical constants (see, e.g., http://physics.nist.gov/cuu/Constants/index.html).

In a scattering event (fig. 1a) the energy of the incident neutron is E_i and that of the scattered neutron is E_f. (The subscripts "i" and "f" mean "initial" and "final" respectively.) Similarly the incident and scattered neutron wave vectors are $\mathbf{k}_i$ and $\mathbf{k}_f$. The "energy transfer" $\hbar\omega = E_i - E_f$ is the energy transferred to the sample by the neutron when it is scattered. Similarly the "wave vector transfer," or "scattering vector," is $\mathbf{Q} = \mathbf{k}_i - \mathbf{k}_f$. The cosine rule, applied to the ($\mathbf{Q}$, $\mathbf{k}_i$, $\mathbf{k}_f$) scattering triangle (fig. 1b), gives $Q^2 = k_i^2 + k_f^2 - 2k_i k_f \cos(2\theta)$, where 2θ is the "scattering angle" (the angle between the incident and scattered neutron beam directions). For the special case of "elastic scattering," i.e., scattering in which the energy of the neutron does not change, $E_i = E_f$, $\hbar\omega = 0$, $k_i = k_f$, and $Q = 2k_i \sin\theta = 4\pi \sin\theta/\lambda_i$ where λ_i is the incident wavelength.

II.2. Basic Theory

In order to understand neutron powder diffraction, and to compare neutron diffraction with x-ray diffraction (Warren, 1969), we shall discuss the basic theory of the method. Detailed treatments are found in books by Bacon (1975), Squires (1978), and Lovesey (1987).

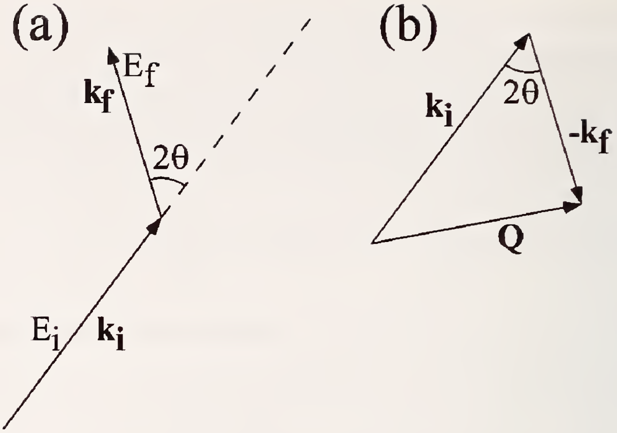

Fig. 1. A scattering event is illustrated (a) in real space: (b) shows the corresponding scattering triangle. The symbols are defined in the text.

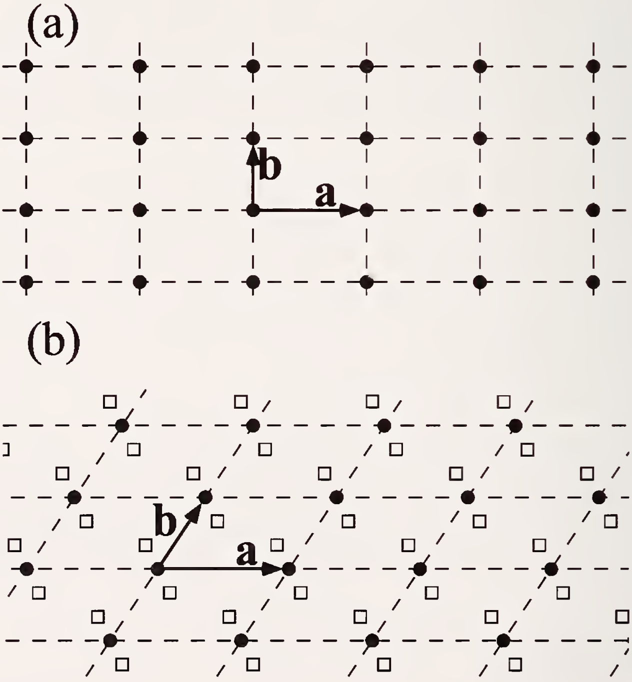

Fig. 2. Unit cells (a) without a basis and (b) with a basis. Two-dimensional examples are shown for simplicity. Real space basis vectors **a** and **b** are shown. With this choice of **a** and **b** the fractional coordinates of the atoms represented by open squares, in (b), are (0.75,0.25) and (0.25,0.75).

The atoms in a crystalline material are periodically arranged. Their positions can be generated by specifying the size and shape of a "unit cell" and the positions of the atoms within the unit cell. The complete structure is obtained by repeating the unit cell many times in all directions. This is illustrated in fig. 2. In a few cases (those of some but not all elements) there is only one atom in the unit cell so that all atomic positions are equivalent and the environment of every atom is the same (fig. 2a). In the vast majority of cases there are several atoms (indeed any number from 2 to many thousands) in the unit cell (fig. 2b). In all cases the crystal structure is described by three real space basis vectors **a**, **b** and **c**, that define the size and shape of the unit cell and by the (equilibrium) positions of the atoms within the cell, which are generally expressed in fractional coordinates (fig. 2).

Neutrons are scattered by nuclei, and by atomic magnetic moments due to unpaired electrons. For now we shall only consider the nuclear scattering. We shall also assume (for the time being) that all unit cells are identical (even to the extent that the atoms do not move), and that complicating effects, such as extinction, absorption, inelastic scattering and multiple scattering, can be ignored.

The scattered intensity in a neutron diffraction experiment is proportional to $I_0NS(\mathbf{Q})$ where I_0 is the incident beam intensity and N is the total number of atoms in the crystal. The structure factor $S(\mathbf{Q})$ is given by

$$S(\mathbf{Q}) = \frac{1}{N}\left|\sum_i^N b_i \exp(i\mathbf{Q}.\mathbf{r}_i)\right|^2 , \qquad (2)$$

where the sum is over all atoms, $\mathbf{r}_i$ is the position of atom i, and b_i is the "scattering length" or "scattering amplitude" for atom i, which is a measure of the strength of the interaction between the incident radiation and the atom. (Values of b_i are readily available, e.g., on the Web at http://www.ncnr.nist.gov/resources/n-lengths/). In a crystalline material the periodicity of the lattice implies that $S(\mathbf{Q})$ is zero except at specific values of $\mathbf{Q}$, such that the phase factors exp $(i\mathbf{Q}.\mathbf{r}_i)$ constructively interfere. These special values of **Q**, plotted in a 3-dimensional space called "reciprocal space," form a regular grid of points known as the reciprocal lattice. Vectors among these points, called "reciprocal lattice vectors," may be written in terms of three reciprocal space basis vectors **a***, **b*** and **c***:

$$\mathbf{G}_{hk\ell} = h\mathbf{a}^* + k\mathbf{b}^* + \ell\mathbf{c}^* . \qquad (3)$$

The "Miller indices" h, k and ℓ are integers which characterize the reflection that occurs when $\mathbf{Q} = \mathbf{G}_{hk\ell}$. These reflections are known as Bragg reflections, and the peaks observed in diffraction experiments (both with crystals and with powders) are generally called Bragg peaks.

The reciprocal space basis vectors are related to the real space basis vectors **a**, **b** and **c**: $\mathbf{a}^* = (2\pi/V)\, \mathbf{b} \times \mathbf{c}$, with cyclic permutations, where $V = \mathbf{a}.(\mathbf{b} \times \mathbf{c})$ is the volume of the unit cell.

The periodicity of the lattice (with the assumption that N is very large) enables us to write equation (2) somewhat differently:

$$S(Q) = \frac{(2\pi)^3}{nV} \sum_G \delta(Q - G) \left| \sum_i^n b_i \exp(iQ.r_i) \right|^2 . \tag{4}$$

The first sum is over all reciprocal lattice vectors; the delta function implies that S(**Q**) is only nonzero when **Q** is a reciprocal lattice vector. The second sum is restricted to the n atoms in a single unit cell.

In a single crystal measurement using a mono-directional monochromatic (single wavelength) incident beam, the incident wave vector $\mathbf{k}_i$ is well defined. Since scattering only occurs when $\mathbf{Q} = \mathbf{G}_{hk\ell}$, and since $\mathbf{k}_f = \mathbf{k}_i - \mathbf{Q}$ (fig. 1a), the scattered neutrons leave from the sample in discrete directions.

In the case of a powder the structure factor must be averaged over all possible crystallite orientations. As long as the dimensions of all crystallites are much greater than those of the unit cell we obtain a simple function of scalar Q, which vanishes except when Q is equal to the magnitude of one of the reciprocal lattice vectors $\mathbf{G}_{hk\ell}$. Since (for elastic scattering) $Q = 4\pi \sin\theta / \lambda_i$ (section II.1), the scattering from a powder sample in an idealized experiment with a mono-directional monochromatic incident beam only occurs at scattering angles 2θ such that $\sin\theta = G_{hk\ell}\lambda_i / 4\pi$, i.e., $\lambda_i = 2d_{hk\ell} \sin\theta$ (which is the familiar Bragg equation), where the distance between diffracting planes is $d_{hk\ell} = 2\pi / G_{hk\ell}$. Because all crystallite orientations are present the scattered neutrons leave from the sample in "Debye-Scherrer" cones.

II.3. Instrumentation

In a conventional neutron powder diffractometer, at a continuous source such as the NIST Research Reactor, a beam of monochromatic neutrons is incident upon a sample and the scattered neutron intensity is measured as a function of the scattering angle 2θ (fig. 3). The monochromatic incident beam is produced by Bragg reflection from an appropriate single crystal monochromator. The neutron count-rate is measured in one or more detectors. Masks and collimators restrict the spatial and angular widths of the beam. In the absence of complicating effects such as those listed previously, and ignoring resolution effects and other sources of unwanted counts such as ambient background and scattering from the sample environment, the neutron count-rate is proportional to $S(Q)/(\sin\theta \sin 2\theta)$, where $S(Q)$ is simply $S(\mathbf{Q})$ summed over all directions of $\mathbf{Q}$ (Squires 1978, page 43).

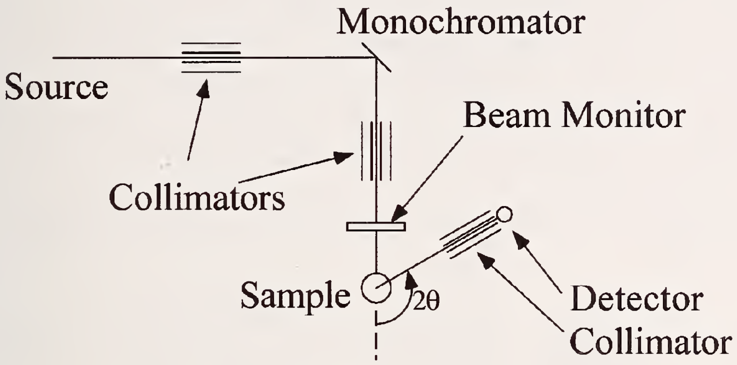

Fig. 3. A schematic drawing of a diffractometer, showing the neutron source, the monochromator crystal, a beam monitor, the sample, and a detector. Collimators are placed before and after the monochromator crystal and between the sample and the detector.

In an ideal experiment the incident beam would have a single wavelength and unique direction, but there would be no intensity at the sample. In practice the incident beam has a narrow distribution of wavelengths and a narrow distribution of directions. The intensity at the sample is roughly proportional to the product of the widths of these distributions whereas the overall resolution of the instrument (assuming its design is optimized) is roughly proportional to one of the widths. Depending on the experiment the compromise between intensity and resolution will vary.

A very different neutron diffraction technique, which we shall not discuss further, is known as "time-of-flight diffraction" (Windsor, 1981). In this case a pulsed source, or a "neutron chopper" at a continuous source, provides pulses of neutrons with a broad spectrum of wavelengths. The neutrons strike a sample and are scattered in various directions, arriving at the detector(s) at times that depend on their wavelengths. Given a detector's scattering angle and its distance from the source, each peak in the time-of-flight spectrum is uniquely associated with one or more Bragg reflections. As before the intensities of the Bragg reflections are used to determine structure factors S(Q).

II.4. The BT1 Spectrometer at the NIST Research Reactor

In 1992 a third generation multipurpose powder diffractometer was installed at the BT1 (beam tube #1) beam port of the NIST Research Reactor (http://www.ncnr.nist.gov/instruments/bt1). Selecting from a choice of three monochromator crystals and two white beam collimators with different acceptance angles (fig. 4), the response of the instrument may be tailored to the needs of the experiment. The resolution in wave vector transfer Q is shown in fig. 5 for the six choices of instrumental setup. The Ge(311) monochromator, which operates with an incident wavelength of 2.0783(2) ≈, yields the highest neutron intensity and best resolution at low Q, but Q is limited to about 6 $\approx^{-1}$. On the other hand Si(531), at 1.5905(1) ≈, provides the best resolution at high scattering angles, but six times longer data collection times are required

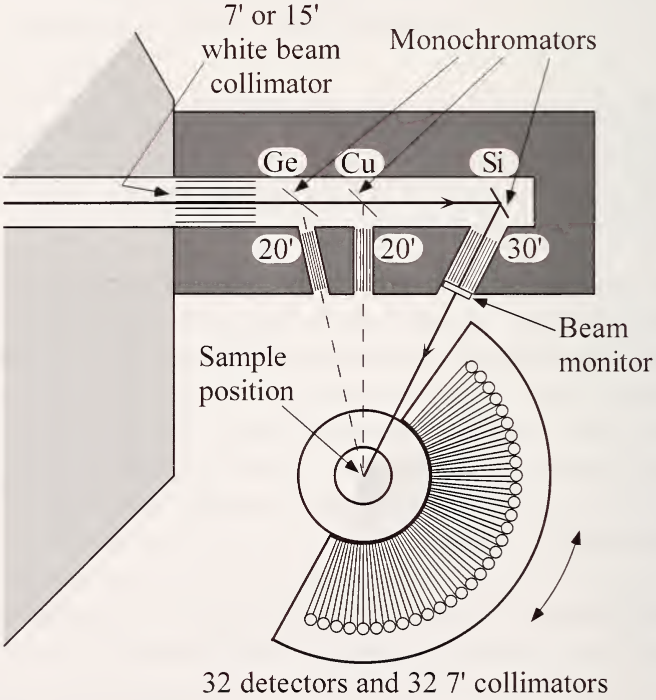

Fig. 4. A schematic drawing of the BT1 diffractometer at the NIST Research Reactor. The beam monitor and the detector assembly are shown in locations appropriate for data collection using the Si(531) monochromator.

because the flux at the sample position is much lower. For most experiments the Cu(311) monochromator, at 1.5402(2) Å, offers the most useful compromise between intensity and resolution, with intermediate data collection times.

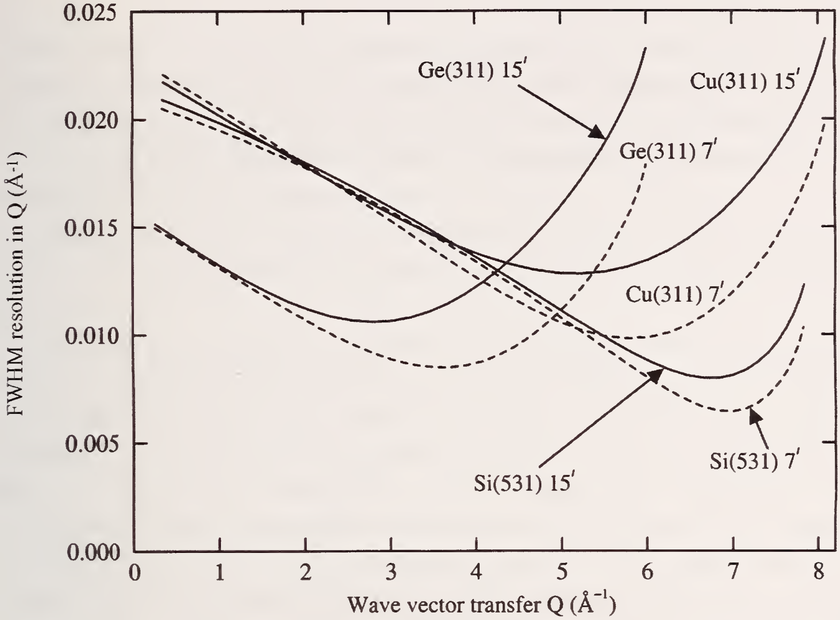

Fig. 5. The FWHM (full width at half maximum height) of the resolution function of the BT1 diffractometer, as a function of Q, for the six possible combinations of monochromator crystal and in-pile collimation.

The BT1 instrument is equipped with an array of 32 detectors located at 5° intervals within a common shield. It also has a low efficiency detector, placed in the incident monochromatic beam to monitor the beam intensity (fig. 4). In a typical experiment the detector assembly is moved to the desired starting position and counts are accumulated in the 32 detectors until a predetermined number of counts has been recorded in the beam monitor. Measurements are repeated and checked for internal statistical agreement. The assembly is then rotated through a small angle (typically 0.05°), and counts are again accumulated, repeated and checked, using the same number of beam monitor counts. This step/count sequence is repeated until the total angle of rotation is at least 5°, so that data from each detector overlap with data from its neighbors. The assembly can be rotated through 13°, and measurements can be made with 2θ from 0° to 167°.

II.5. Scattering of Neutrons and X-rays

The discussion of section II.2, with the same simplifying assumptions, also applies to x-ray diffraction.

In comparing the two techniques the first remark to be made is that the scattered intensity is generally much greater for x-rays than for neutrons because the source is much more intense. Hence x-ray diffraction is an extremely powerful technique that is frequently preferable to neutron diffraction. Nevertheless there are many situations where the neutron technique is superior and/or complementary in the sense that new information can be obtained by combining the results of measurements using the two techniques.

An important difference between x-rays and neutrons is in the nature of the interaction between probe and sample. The neutron-nucleus interaction is of very short range (of order 10^{-15} m), very much shorter than interatomic distances (which are of order 10^{-10} m), so that scattering lengths b are essentially independent of Q over the range of Q values accessible in a neutron scattering experiment. On the other hand x-rays interact with electrons and since the spatial extent of the electron cloud surrounding a nucleus is comparable with interatomic distances the corresponding quantity, known as the "form factor," decreases quite quickly with increasing Q (fig. 6). This quantity, which we shall write as f(Q), is the Fourier transform of the radially averaged density of electrons surrounding the nucleus. The decrease in f with increasing Q can

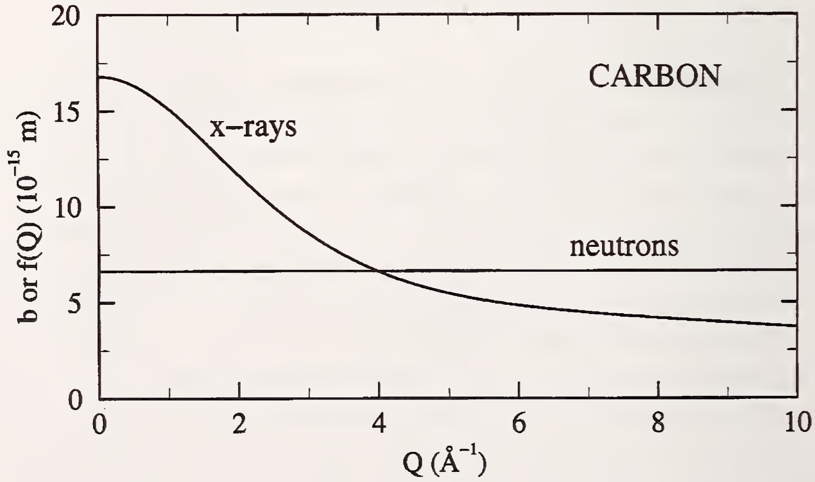

Fig. 6. The neutron scattering length of carbon, b, which is independent of Q, and the corresponding x-ray atomic scattering factor, f(Q).

cause problems in x-ray experiments when there is significant background scattering such as Compton (incoherent) scattering, either from the sample or from the sample environment, since the ratio of signal to background is greatly reduced at high angles. A more fundamental distinction is that x-rays provide information about the electron density distribution in a material whereas neutrons give nuclear positions. Thus qualitatively different information can be extracted from the two probes. It is not always the case that nuclear positions can be derived from electronic density distributions and of course the converse never applies.

Another difference between x-rays and neutrons is that for x-rays the forward scattering value of f(Q), i.e., f (0), is proportional to the number of electrons, i.e., to the atomic number Z, whereas for neutrons there is no simple relationship between the equivalent quantity, b, and the composition of the scattering nucleus. Indeed b varies somewhat erratically with Z, as illustrated in fig. 7. Thus neutrons can sometimes be used to distinguish among elements that are close to one another in the periodic table and therefore barely distinguishable in x-ray experiments; an example occurs in the study of zeolites containing Al ($Z=13$, $b=3.5\times10^{-15}$ m) and Si ($Z=14$, $b=4.2\times10^{-15}$ m). Furthermore it is frequently easier to detect light atoms in the presence of heavy atoms using neutrons rather than x-rays; light elements with significant scattering lengths include the common elements H, C, N and O.

The neutron-nucleus scattering length also depends, sometimes dramatically, on the isotope whereas f(Q) does not since x-rays are scattered by electrons. The best known example of the isotope dependence of b involves H and D, whose scattering lengths are -3.8×10^{-15} m and $+6.7\times10^{-15}$ m respectively, whereas the value of f(0) is 2.8×10^{-15} m (for both isotopes). The isotope dependence of b has been used to particular advantage in small angle scattering studies of polymers and biological materials and in studies of partial distribution functions in liquids and dense gases. There have been a few reports of the use of isotope substitution in powder diffraction studies.

II.6. Absorption of Neutrons and X-rays

With very few exceptions, x-rays are much more strongly absorbed than neutrons. For example the 1.8 Å x-ray and neutron linear absorption coefficients for aluminum are $\approx 21\ \mathrm{mm}^{-1}$ and $\approx 0.0014\ \mathrm{mm}^{-1}$ respectively. Thus at this wavelength a 150 mm thick aluminum plate has about the same transmission for neutrons as that of a 10 μm thick plate for x-rays (≈ 80%).

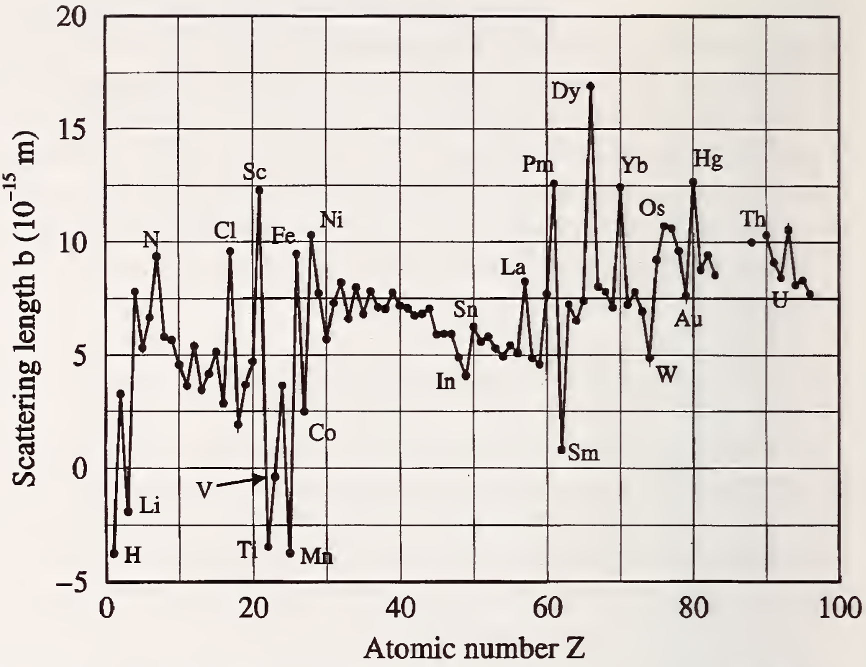

Fig. 7. The real part of the neutron scattering length b for the naturally occurring elements.

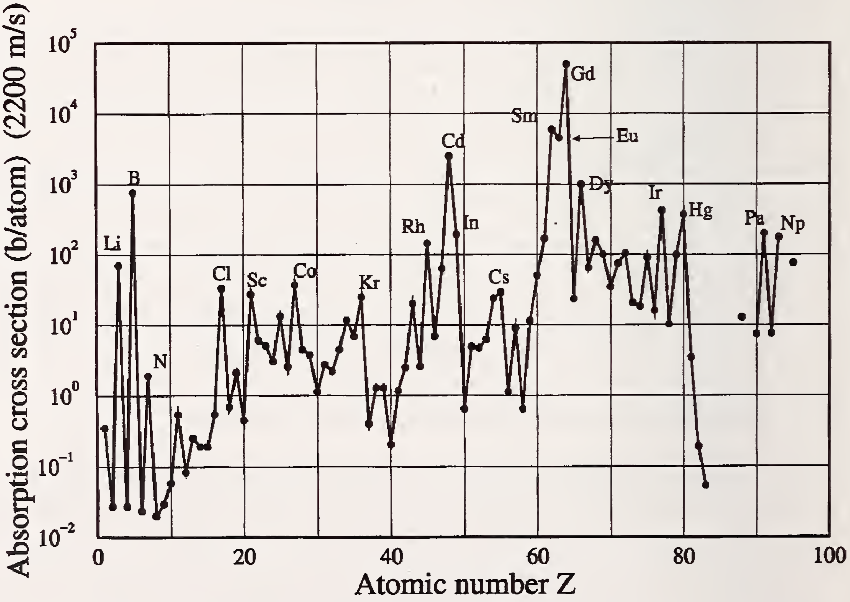

Fig. 8. The absorption cross section for 2200 m/s neutrons for the naturally occurring elements. Notice that the ordinate is plotted on a log scale.

Absorption probabilities are written in terms of microscopic or macroscopic absorption cross sections, denoted by σ_{abs} and Σ_{abs} respectively. The probability of neutron absorption by nuclei of a given element, within an infinitesimal distance x, is simply $\rho\sigma_{abs}x$ or $\Sigma_{abs}x$, where ρ is the macroscopic number density of nuclei of that element. (Note that the macroscopic number density of nuclei is the product of the crystallographic number density and the powder packing fraction, which is typically of order 65 %.) The microscopic cross section σ_{abs} is the more fundamental quantity since it is a cross section per atom; the macroscopic cross section $\Sigma_{abs} = \rho\sigma_{abs}$ is a cross section per unit volume so it depends on the material in which the element is found. The macroscopic absorption cross section of a material is simply the sum of contributions from each of its constituent elements. Microscopic cross sections are normally expressed in barns (abbreviation "b"), a unit that is "temporarily accepted for use with the [International System of Units,] SI" (Taylor 1995); $1\ \text{b} = 10^{-24}\ \text{cm}^2 = 10^{-28}\ \text{m}^2$. The microscopic absorption cross sections of the natural elements are shown in fig. 8. Once again there are wild fluctuations from one element to the next: neutron absorption cross sections span roughly six orders of magnitude. They also vary, sometimes greatly, from one isotope to another. For example σ_{abs} = 940 b/atom for ^{6}Li but only 0.045 b/atom for ^{7}Li.

Neutron diffraction experiments on materials containing elements with a large absorption cross section (e.g., Li, B, Cd, Gd, Sm, Eu, ...) are generally more challenging because the scattering is greatly reduced and a significant absorption correction may be necessary. In addition there are safety concerns because both prompt and delayed γ-radiation are produced; a notable exception is lithium. If the sample contains a strong absorber extra shielding may have to be placed to protect personnel, and it may be necessary to let the sample's activity decay for days, if not weeks or months, before it can be removed from the site without special handling. All such matters must be discussed with the appropriate authorities in advance of the proposed experiment. Potential problems can sometimes be avoided by using samples containing elements that have been depleted of the offending isotope. For example a sample made with ^{112}Cd (σ_{abs} = 2.2 b/atom) or ^{114}Cd (σ_{abs} = 0.34 b/atom) is clearly better than a sample made with natural Cd (σ_{abs} = 2520 b/atom), but it may be very expensive. On the other hand many isotopes are separated for medical purposes and some of these isotopes may be relatively inexpensive, so it is prudent to research prices before dismissing an isotope substitution experiment out of hand.

A comprehensive list of absorption cross sections may be found on the Web at http://www.ncnr.nist.gov/resources/n-lengths/.

Absorption cross sections depend on the energy of the neutron whereas the scattering cross sections σ_C and σ_I, to be introduced in the following section, do not. For most elements and isotopes σ_{abs} is directly proportional to the neutron wavelength but there are important exceptions such as the strong absorbers Cd and Gd. When single values of σ_{abs} are tabulated they are most commonly (but not always) quoted for the canonical thermal neutron speed of 2200 m/s, which corresponds to a wavelength of approximately 1.8 Å.

The ability of neutrons to penetrate deep within materials can be an important advantage. In studies of materials with compositional gradients, such as cast ingots and coatings, neutron diffraction yields a structure that is representative of the bulk material whereas x-rays provide less useful information, regarding the crystal structure very close to the surface. The ability of neutrons to penetrate materials also opens up the possibility of measuring residual stresses within thick samples; we shall briefly return to this subject in section III.3.

A second important consequence of the low absorption of neutrons is that sample environments for neutron experiments are relatively easy to design, since neutron beams readily penetrate the various structures that surround the sample in devices such as cryostats, furnaces and even high pressure cells; some examples are shown in figs. 9-11. Information about sample environments available at the NIST Center for Neutron Research may be found at http://www.ncnr.nist.gov/equipment/ancequip.html.

II.7. Incoherent Scattering

In our discussion of the basic theory we assumed that all unit cells were identical. To the extent that this is untrue the expressions given in section II.2 are not entirely correct. We shall use the word "disorder" to describe situations that cause unit cells to differ from one another, and in this section we shall discuss two types of nuclear disorder. Various kinds of atomic disorder will be discussed in section II.8.

Consider a material that contains one or more elements with more than one stable isotope. Since neutron scattering lengths depend both on Z and on the isotope, the unit cells in this material are not identical and our expression for S(**Q**) must be modified. For example eq. (2) becomes

$$S(Q) = \frac{1}{N}\left\{\left|\sum_{i}^{N}\langle b_i\rangle \exp(iQ.r_i)\right|^2 + \sum_{i}^{N}\left[\langle b_i^2\rangle - \langle b_i\rangle^2\right]\right\}, \qquad (5)$$

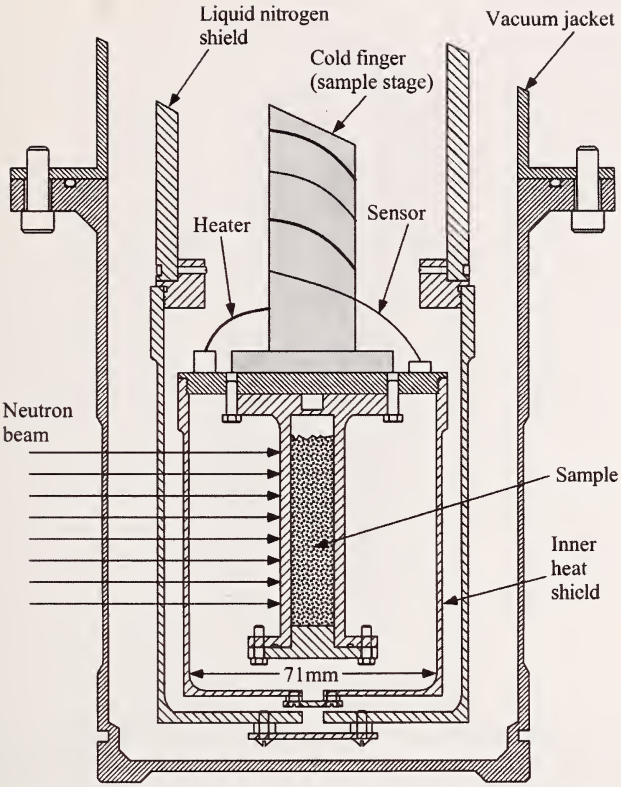

Fig. 9. A popular low temperature setup, enabling sample temperatures down to of order 10 K. The sample is bolted to the cold stage of a closed cycle helium refrigerator. There are two heat shields and an outer vacuum vessel, all made of aluminum.

where angle brackets denote averages over isotopic distributions. The first term in this equation is the Bragg scattering, which is "coherent" and of course strongly dependent on Q. The second term, which is independent of Q, is "incoherent" scattering. The strength of the incoherent scattering due to any given type of atom is proportional to the variance of its scattering length.

Since the neutron has a spin of ½, the interaction of a neutron with a nucleus with nonzero spin I depends on the spin state of the compound nucleus, which is either I+½ or I-½. To the extent that the distribution of nuclear spin directions in a material is random, this produces an additional type of incoherent scattering, which is again independent of Q. Equation (5) still applies, but the angle bracket averages now include nuclear spin states as well as isotopes. The quantities $\sigma_C = 4\pi \langle b\rangle^2$ and $\sigma_I = 4\pi [\langle b^2\rangle - \langle b\rangle^2]$ are called coherent and incoherent scattering cross sections respectively. In analogy with our earlier

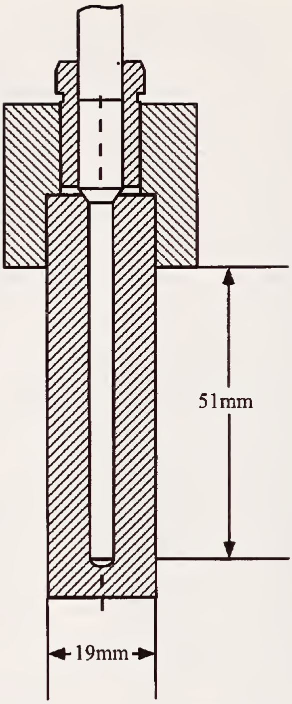

Fig. 10. A schematic drawing of a high pressure cell, made of a high strength aluminum alloy and capable of operating pressures up to ≈ 620 MPa (≈ 6100 atmospheres).

discussion of absorption the probability of incoherent scattering by atoms of a given element whose incoherent scattering cross section is σ_I, within an infinitesimal distance x, is simply $\rho\sigma_I x$. On the other hand no such simple expression applies to coherent scattering. The coherent scattering probability depends, inter alia, on the structure of the material and on the incident neutron wavelength. Beyond the so-called Bragg cutoff wavelength λ_c, which is such that the Bragg equation $\lambda_i = 2d_{hk\ell} \sin \theta$ cannot be satisfied for $\lambda_i > \lambda_c$, there is no coherent scattering whatsoever (neglecting atomic disorder). Furthermore the coherent scattering probability for a single crystal clearly depends on its orientation with respect to the incident beam; there is no coherent scattering unless **Q** is equal to a reciprocal lattice vector.

Most elements are predominantly coherent scatterers. The most important exceptions are hydrogen and vanadium. The spin-incoherent scattering cross section of hydrogen, which is ≈ 80 b/atom in a hypothetically bound material, is a nuisance in diffraction studies since it contributes a large constant background to the measured intensity. For this reason deuterated samples are

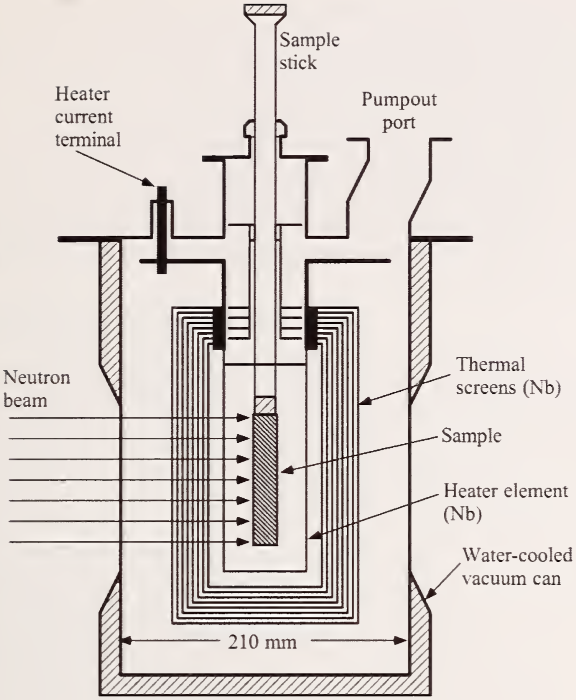

Fig 11. A schematic drawing of an 1800 °C furnace, designed at the Institut Laue-Langevin, Grenoble, France. At beam height the heater consists of two concentric 0.02 mm thick Nb foils, the eight heat shields are also 0.02 mm Nb foils, and the outer vacuum jacket is made of ≈1.5 mm thick aluminum.

strongly recommended. Since vanadium (at natural abundance) scatters almost completely incoherently, it is frequently used to make sample containers for powder diffraction experiments; the weakness of its Bragg peaks, due to its very small coherent scattering cross section, is a major advantage which outweighs any disadvantage associated with the incoherent scattering background. On the other hand it is difficult to determine the positions of V atoms in a sample because of its very small coherent scattering cross section.

II.8. Atomic Disorder

At least one type of atomic disorder is never absent, no matter how carefully the sample is prepared. This is the thermal disorder that is associated with the motion of atoms about their mean positions. The effect on the scattering is to shift a certain amount of intensity from the Bragg peaks to scattering that is continuous in Q (whereas Bragg scattering occurs at discrete values of Q). The continuous scattering is sometimes called "thermal diffuse scattering." If the thermal motion is isotropic Bragg intensities are modified by replacing b_i with $b_i \exp(-\frac{1}{2}Q^2\langle u_i^2\rangle)$, where the exponential expression is the so-called "temperature factor," or "Debye-Waller factor," for atom i; $\langle u_i^2\rangle$ denotes the atom's mean square displacement. The temperature factor may also be written as $\exp(-B_i[\sin\theta / \lambda]^2)$, where B_i is the "displacement parameter" for atom i. In many cases the thermal motion is anisotropic, in which case temperature factors are considerably more complicated (Willis and Pryor, 1975). Displacement parameters are routinely obtained in the analysis of powder diffraction experiments.

Other kinds of atomic disorder modify the scattered intensity in a diffraction experiment (Guinier, 1963). They include local effects such as compositional disorder, vacancies and interstitials, as well as more extended phenomena such as dislocations, grain boundaries, clusters and pores. The larger scale structures are generally better studied using the small angle scattering technique whereas smaller scale objects show up better in diffraction experiments. Defects generally modify the Bragg scattering and contribute to the diffuse scattering between the Bragg peaks. The Bragg peaks may be modified in intensity, position and/or width, and the different ways that these modifications depend on the reflection can be used to distinguish among the various phenomena. For example line broadening can be due to the small size of the crystallites in the sample, in which case it is independent of Q, or it can be due to the effects of strains, in which case it increases with increasing Q.

II.9. Magnetic Scattering

We have seen that neutrons interact with nuclei. Because of their magnetic moment they also interact with magnetic moments on atoms with unpaired electrons (Furrer 1995). The magnetic interaction of neutrons is more complicated than the nuclear interaction, and we shall only consider the simplest of situations. For a detailed discussion see Izyumov and Ozerov (1970).

A crystalline material with an ordered magnetic structure (e.g., a ferromagnetic or anti-ferromagnetic material), placed in a neutron beam, produces magnetic Bragg peaks in addition to the nuclear Bragg peaks previously discussed. If the beam is unpolarized the nuclear and magnetic structure factors, $S(\mathbf{Q})$ and $S_M(\mathbf{Q})$, add in the following way:

$$S_{tot}(\mathbf{Q}) = S(\mathbf{Q}) + S_M(\mathbf{Q})\sin^2\alpha, \tag{6}$$

where α is the angle between the magnetization vector $\mathbf{M}$ and the scattering vector $\mathbf{Q}$. The expression for $S_M(\mathbf{Q})$ is similar to equation (2), except that b_i is replaced with the quantity $p_i(Q) = A_i f_i^M(Q)$ where A_i is proportional to the magnetic moment of atom i and $f_i^M(Q)$ is its magnetic form factor. For a powder the coefficient $\sin^2 \alpha$ is replaced by its average value, which is 2/3.

In some cases (depending on the crystal symmetry), powder diffraction experiments with unpolarized neutrons can be used to determine magnetic structures as well as conventional crystal (chemical) structures. Magnetic moments can also be determined.

II.10. Rietveld Profile Refinement

The standard method of analyzing the results of a neutron powder diffraction experiment, known as "Rietveld profile refinement" and named for Hugo Rietveld (who developed the method), is to fit the parameters of a model to the measured "profile," which is the intensity measured as a function of scattering angle 2θ. A typical measurement and the fitted profile are shown in fig. 12. The Rietveld technique is discussed in Young (1993). See http://www.ncnr.nist.gov/programs/crystallography/ for information about its implementation at the NIST Center for Neutron Research.

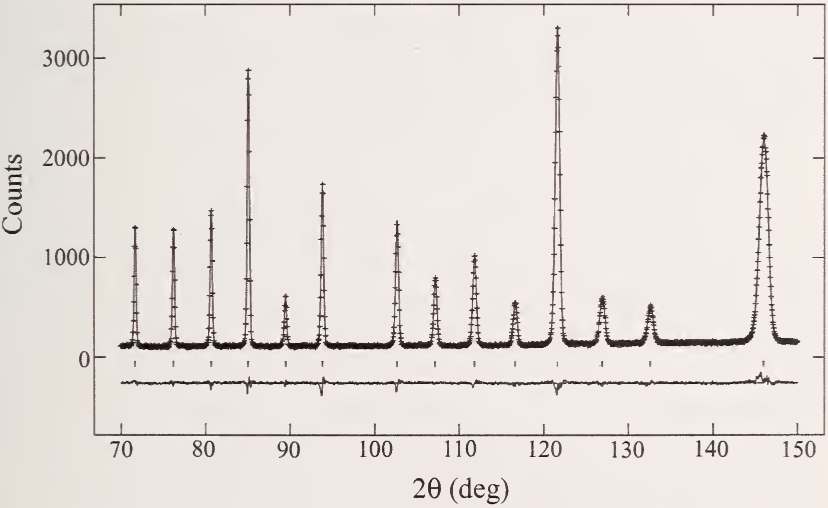

Fig. 12. The high angle part of the neutron powder diffraction pattern of cubic $LaBa_2Fe_3O_{9-\delta}$, measured at 295 K. The incident wavelength was 1.54 Å, obtained using a Cu(311) monochromator. Notice that the widths of the peaks, which are very largely due to the resolution of the instrument, depend on the scattering angle 2θ. Points represent the data and the line through the data represents the result of the profile refinement. The difference between experiment and calculation is shown at the bottom, and the small vertical lines indicate the positions of the calculated peaks.

The model parameters in a Rietveld refinement can be divided into several categories, according to which aspect of the profile they describe. First of all, and most importantly, there are the parameters that determine the positions and integrated intensities of the Bragg peaks. Unit cell parameters determine peak positions whereas atom positions within the unit cell, site occupancies and displacement parameters collectively determine integrated intensities. Next there are parameters that describe the so-called "background," which is the relatively smooth scattering that lies between and below the Bragg peaks. This can include diffuse elastic coherent scattering and inelastic and/or incoherent scattering from the sample and its environment, plus the "true" background, which includes contributions due to air scattering, electronic noise, and other unwanted sources. The Bragg peaks, which correspond to elastic scattering that occurs at well-defined scattering angles, can usually be separated from the background because the background scattering varies rather slowly with scattering angle whereas the Bragg scattering is highly structured. A third set of parameters describes the shapes of the peaks. Line broadening is in part due to the resolution of the instrument itself, which is generally a well-parameterized function of 2θ for a given instrumental configuration. There may also be contributions to the broadening due to size and strain effects. The results of neutron diffraction experiments at a reactor are generally easier to refine than results from other sources because peak shapes tend to be simpler and fewer corrections need be applied.

III. EXAMPLES

We now discuss some examples of applications of the neutron diffraction technique to materials of industrial interest. We conclude with a brief discussion of neutron experiments on C_{60}.

III.1. High Temperature Superconductors

It goes without saying that there is great interest in the development of high temperature superconductors for commercial applications. Neutron diffraction has played a very important role in elucidating the structures of these materials, in large part because of the crucial part played by the oxygen vacancies and the greatly improved visibility of oxygen in the presence of heavy elements when compared with x-ray diffraction. Furthermore the ability of neutrons to penetrate bulk samples, with very little absorption, simplifies the data analysis considerably. Structural information from neutron scattering experiments has helped us improve our understanding of the crucial role of the oxygen defects in high temperature superconductors.

The mercury superconductors $HgBa_2Ca_{n-1}Cu_nO_{2n+2+\delta}$ have generated considerable interest in the superconductivity community. The oxygen dependence of the structure of the single layer material $HgBa_2CuO_{4+\delta}$, with $0.04 \leq \delta \leq 0.23$, and its effect on the superconducting phase transition, have been studied using the neutron powder diffraction method (Huang et al., 1995). The measurements were performed using the BT1 diffractometer at NIST (section II.4). The Cu(311) monochromator was used with 15' in-pile collimation (cf. figs. 4 and 5). The powders, in amounts of the order of 4 g, were contained in thin-walled (0.15 mm) vanadium cans which were mounted in a closed cycle helium refrigerator (cf. fig. 9). Counting times were roughly 8 h at each temperature. The crystal structure (fig. 13) remains tetragonal over the whole range of δ, and at all temperatures from 10 K to 300 K. The excess oxygen is found to occupy so-called O(3) sites in the Hg layers. The displacement parameters for the Hg and Ba atoms are highly anisotropic, such that the corresponding real space displacement ellipsoids (which characterize the probability of finding an atom at a particular location relative to its equilibrium position) are respectively oblate (squashed) and prolate (egg-shaped). This finding suggests that the positions of the Hg and Ba atoms are strongly influenced by the presence or absence of an oxygen atom at the O(3) site. With regard to the Ba atoms, the conjecture is confirmed by results for the distances of the Ba atoms from various oxygen sites in the structure, and by the success of a model that postulates two partially occupied Ba sites at slightly different distances from the Cu planes, such that the sum of the occupancies is unity.

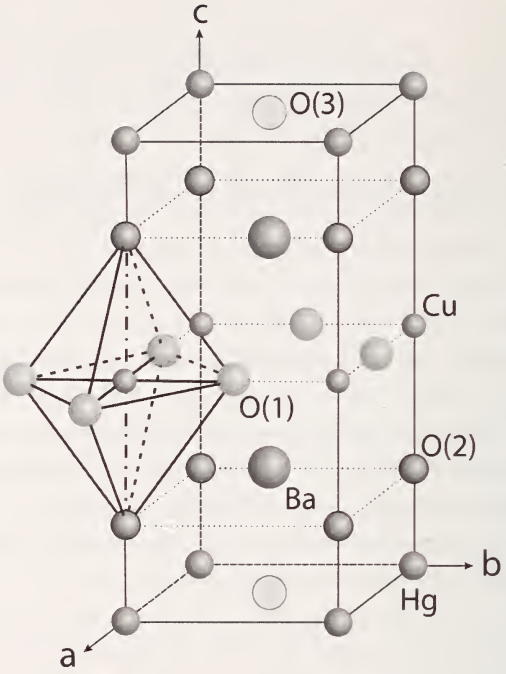

Fig. 13. The tetragonal crystal structure of $HgBa_2CuO_{4+\delta}$. Doping occurs at the partially occupied O(3) sites.

The ratio of the Ba displacement parameters B_{33}(Ba) and B_{11}(Ba), respectively normal and parallel to the tetragonal planes, is shown in fig. 14(a) as a function of δ. This curve is remarkably similar to a plot of the superconducting transition temperature T_c as a function of δ (fig. 14b), suggesting a correlation between T_c and the displacements of the Ba atoms.

III.2. Colossal Magnetoresistors

The resistivity of a magnetic material changes when it is placed in a magnetic field. The effect is generally small, and best observed at low temperature. In some materials the effect is anisotropic, i.e., the resistance changes when the current flowing through the material is changed from being parallel to the internal magnetization to being perpendicular to it. Typically the change in resistance on changing the current direction is of order 1 % or 2 % at most. A good example is permalloy ($Ni_{0.8}Fe_{0.2}$), where the anisotropic magnetoresistance effect is used in device applications such as read heads for computer hard disk drives.

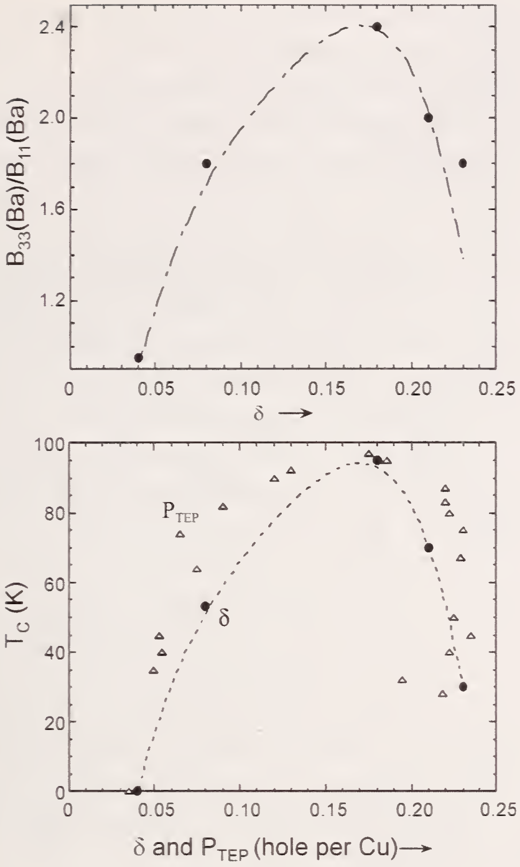

Fig. 14. (a) The ratio of the out-of-plane (B_{33}) and in-plane (B_{11}) displacement parameters for the Ba atoms in $HgBa_2CuO_{4+\delta}$. (b) The dependence of the superconducting transition temperature T_c on δ for $HgBa_2CuO_{4+\delta}$. Also shown is the dependence of T_c on the hole concentration P_{TEP} (the number of carriers per Cu atom), from measurements by Xiong et al. (1994).

About 10 years ago a much larger effect, dubbed "giant magnetoresistance" (GMR), was discovered in an iron-chromium magnetic superlattice. GMR materials have alternating layers of ferromagnetic and non-magnetic metals deposited on an insulating substrate, and the resistance parallel to the layers is largest (its value is R_0) when the magnetic moments in the ferromagnetic layers alternate from one layer to the next (in the absence of an applied field). On the other hand the resistance is smallest (R_∞) when the layers are parallel to one another (when the field saturates the magnetization). In the past few years GMR research has advanced rapidly, with new materials being developed; the current record for the resistance ratio R_0/R_∞ is ≈3.2. Much of the recent GMR research has been driven by a desire to develop a new generation of read heads for computer hard disk drives. A continuing challenge is to manufacture devices that can read increasingly high bit densities. Other types of devices that are candidates for development using GMR materials include magnetic memory chips, magnetic transistors, motion sensors, and sensor arrays for land mine detection.

A somewhat different phenomenon, called "colossal magnetoresistance" (CMR), was first reported in 1994. CMR materials have truly enormous resistance ratios, some being well in excess of 1000. Indeed the change in resistance that occurs when a CMR material is placed in a sufficiently high magnetic field is greater than the change produced when a high temperature superconductor is cooled through its superconducting transition temperature! The resistance of a CMR material drops enormously when the spins order ferromagnetically, either when the temperature is lowered or when a magnetic field is applied. This large variation in carrier mobility originates from a metal-insulator transition that is closely associated with the magnetic ordering. The most well-known CMR materials are the calcium-doped lanthanum manganites $La_{1-x}Ca_xMnO_3$, and the compound with $x=0.33$, which we may write as $La^{3+}_{0.67}Ca^{2+}_{0.33}Mn^{3+}_{0.67}Mn^{4+}_{0.33}O_3$, shows the most dramatic magnetoresistance effect. The undoped material, $LaMnO_3$, is antiferromagnetic but it can be converted to a ferromagnet in an oxidizing atmosphere. This is also true of materials with small x, but at larger values of x the materials are ferromagnetic, no matter how they are prepared.

Much of our understanding about the relationship between the magnetoresistive properties of these materials and their structures has come from neutron powder diffraction experiments. The experiments that we shall briefly describe were part of a comprehensive study of the crystal and magnetic structures of $La_{1-x}Ca_xMnO_3$ compounds with $0<x\leq0.33$. In order to resolve a discrepancy regarding the magnetic ordering in low concentration Ca-doped manganites, Huang et al. (1997) looked at two such materials with $x=0.06$. The first sample, which we shall call the oxidized sample, was prepared in air at 1350 °C by mixing appropriate quantities of La_2O_3, $MnCO_3$ and $CaCO_3$. The other sample, described as reduced, was prepared from the first sample by annealing at 900 °C in a reducing atmosphere. The reduced sample, whose chemical formula may be written as $La_{0.94}Ca_{0.06}Mn^{3+}_{0.94}Mn^{4+}_{0.06}O_3$, had all atomic sites fully occupied whereas the oxidized sample had cation vacancies; its approximate chemical formula was $(La_{0.94}Ca_{0.06}Mn^{3+}_{0.69}Mn^{4+}_{0.31})_{0.96}O_3$. The reduced sample was antiferromagnetic at low temperatures, in common with

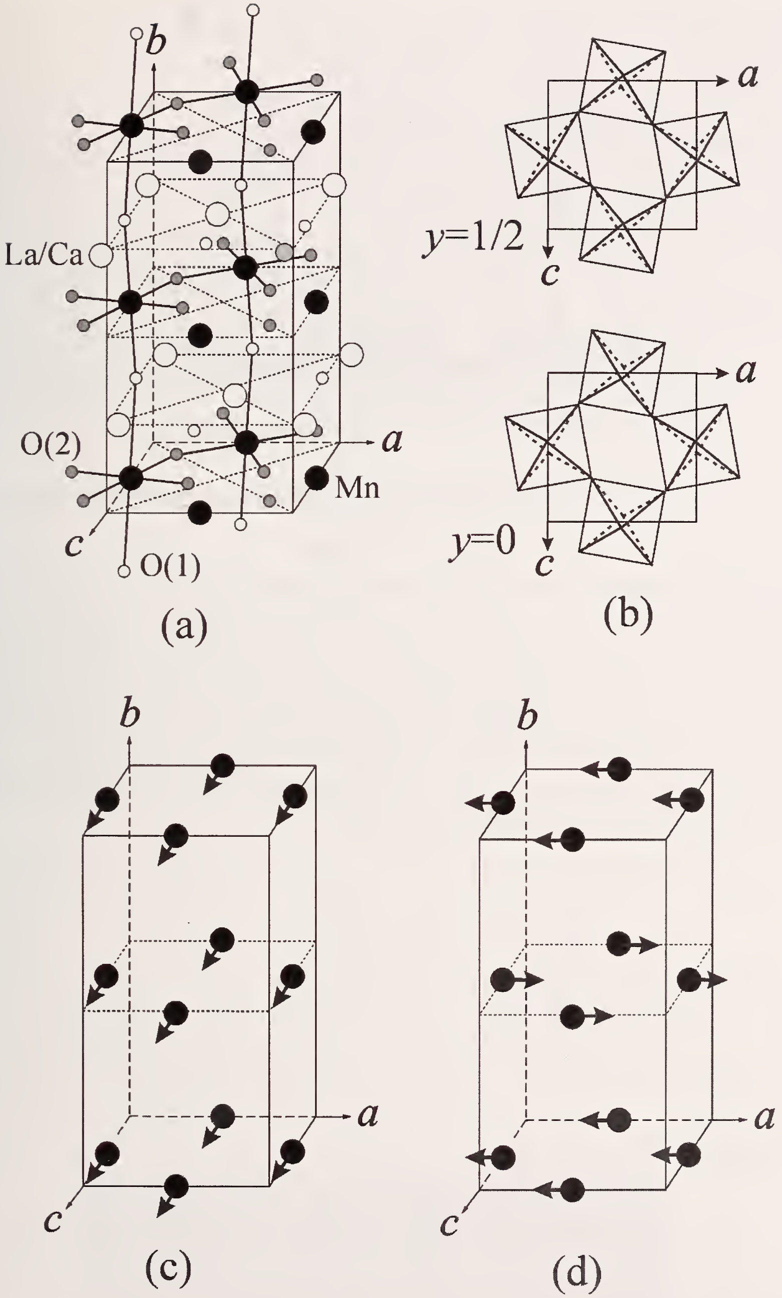

Fig. 15. The orthorhombic crystal structure of $La_{1-x}Ca_xMnO_3$ is shown in (a) and the tilting of the MnO_6 octahedra is shown in (b). The orientations of the Mn magnetic moments are shown in (c) and (d) for the ferromagnetic and antiferromagnetic structures respectively.

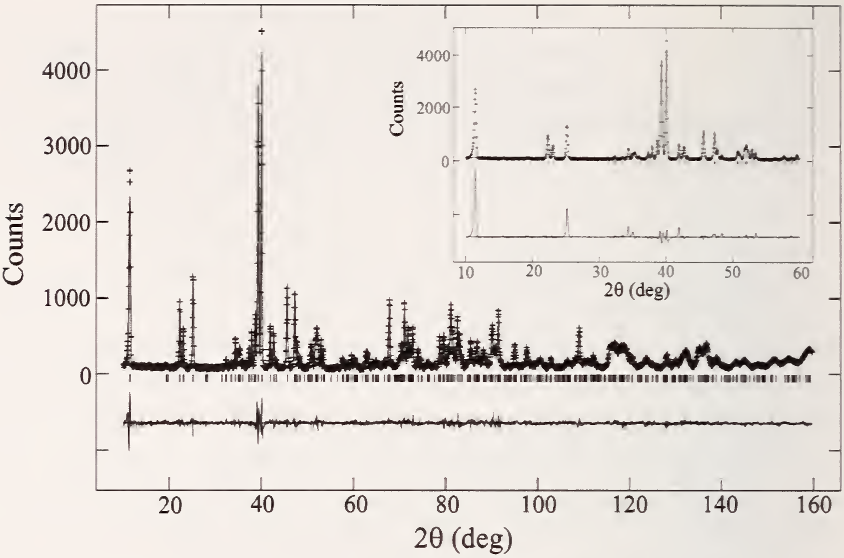

Fig. 16. Rietveld refinements using neutron diffraction data for the stoichiometric reduced compound $La_{0.94}Ca_{0.06}MnO_3$ at 12K. The points are the data and the line through the points is the result from the refinement. The Bragg peak positions are shown as short vertical lines. At the bottom is shown the difference between the data and the calculated profile. The inset shows the low angle data together with the calculated profile for the nuclear contribution to the diffraction pattern; the magnetic contribution shows up in the difference plot at the bottom of the inset.

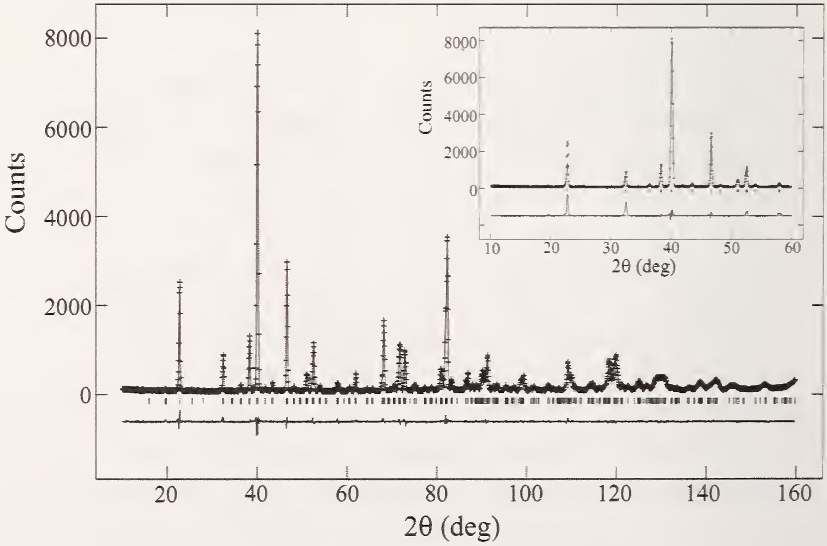

Fig. 17. Rietveld refinements for the oxidized compound $(La_{0.94}Ca_{0.06})_{0.96}Mn_{0.96}O_3$ at 12 K. See the caption to figure 16.

the undoped compound $LaMnO_3$, but the oxidized sample was ferromagnetic, since a far greater proportion of the Mn ions were in the +4 valence state. The orthorhombic crystal structure is illustrated in fig. 15, together with the magnetic ordering in the ferromagnetic and antiferromagnetic states. Figs. 16 and 17 show refinements of the structures of the reduced and oxidized compounds. In each of these figures the upper part of the inset shows the low angle data, represented by symbols, and the calculated profile for the crystal structure alone. The lower part of each inset shows the difference, which represents the magnetic scattering. We see from these figures that the reduced compound has peaks that are purely magnetic whereas the oxidized sample does not. The oxidized compound is ferromagnetically ordered as in fig. 15(c), whereas the reduced sample is antiferromagnetically ordered as in fig. 15(d).

III.3. Residual Stress Measurements

One of the best examples of an applied research area that benefits from neutron diffraction is the study of residual stresses in materials (Prask and Brand, 1997). The neutron method is non-destructive and capable of relatively deep penetration within many materials. The non-destructive nature of the technique is especially important because the act of cutting into a material in order to perform a destructive measurement can actually modify the stresses that the measurement was intended to determine.

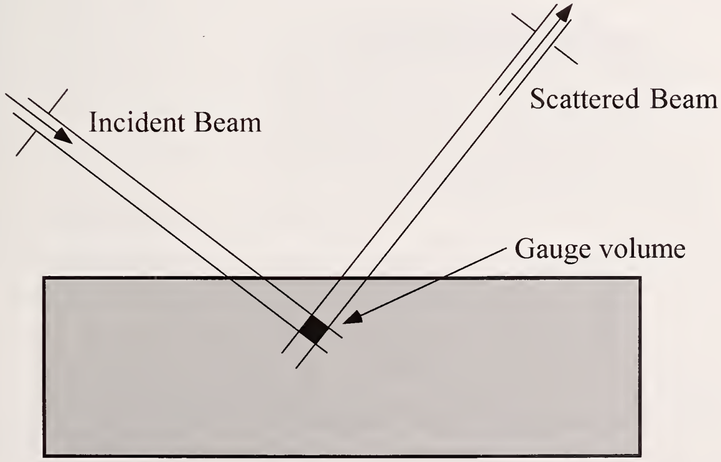

Fig. 18. A schematic representation of the experimental setup for a residual stress measurement. The incident and scattered beams are well collimated and spatially restricted using neutron-absorbing masks.

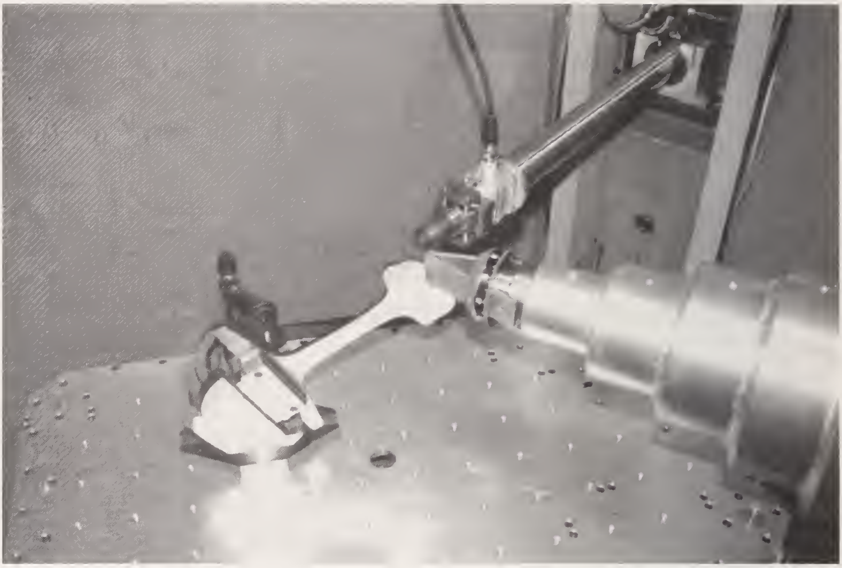

Fig. 19. The actual experimental setup for the determination of residual stresses in a slice of railroad rail, using the BT8 spectrometer at the NIST Research Reactor. The incident beam tube is at the top and the collimation system for the diffracted neutrons is at the lower right of the picture.

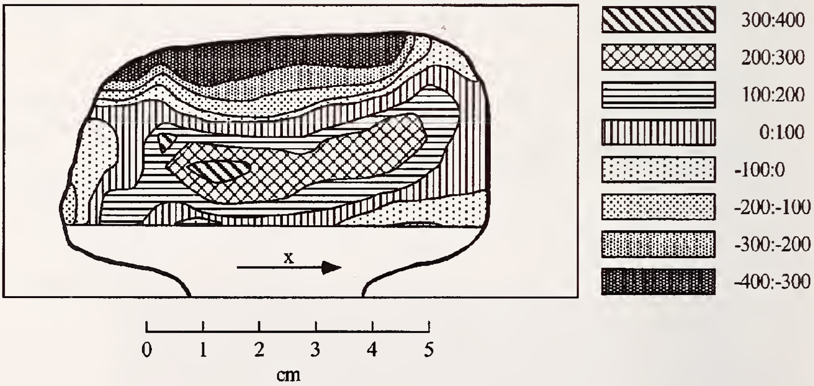

Fig. 20. A contour map showing the residual stress σ_{xx} in the rail head as a function of position. Stresses are in MPa. Positive values are tensile; negative values are compressive.

A typical experimental setup is shown in fig. 18. The incident and diffracted beams are not only well collimated (restricted in direction) but also limited in lateral extent using neutron-absorbing masks. Thus the only once-diffracted neutrons that can enter the detector are those that were scattered within a "gauge volume" defined by the intersection of the incident and diffracted beams. The optimum setup occurs when the scattering angle is 90º: for fixed widths of the incident and scattered beams the irradiated volume is proportional to $1/\sin(2\theta)$, which is minimized when $2\theta = 90°$. By translating the sample within the beam, different gauge volumes can be examined.

Residual stresses are not directly measured in these experiments (nor using any other experimental technique). Writing the Bragg equation as $\lambda = 2d\sin\theta$, the mean lattice spacing within the gauge volume, d, is determined from the angular position of the observed Bragg peak. The local strain is $(d-d_0)/d_0$, where d_0 is the unstressed lattice spacing. Stresses are computed using the diffraction elastic constants for the reflection.

Many residual stress studies have been undertaken over the past 15 years, and dedicated facilities are now found at neutron scattering centers in North America, Europe and Asia. Systems that have been studied include weldments, ceramic coatings, composites, reference specimens, turbine blades, and various military components. An example that illustrates the technique is a recent study of residual stresses in a thin (6.35 mm thick) section of railroad rail (Brand et al., 1996). The experimental setup is shown in fig. 19. Measurements were made using a ≈2.4 mm ×2.4 mm ×2.4 mm gauge volume, at a mesh of points that were 5 mm apart in orthogonal x and y directions normal to the length of the uncut rail. Measurements of 5 different lattice spacings, in five different orientations at each of the mesh points, were used to extract four components of the residual stress tensor. A typical result is shown in fig. 20.

The results of these types of experiments are typically compared with the results of model calculations, enabling engineers to improve their models. They are also compared with the results of other types of experimental investigations, some of which may have the advantage that they are relatively inexpensive though they may not be as accurate. The ultimate objective is to be able to predict performance with reasonable accuracy, thereby improving economy and durability.

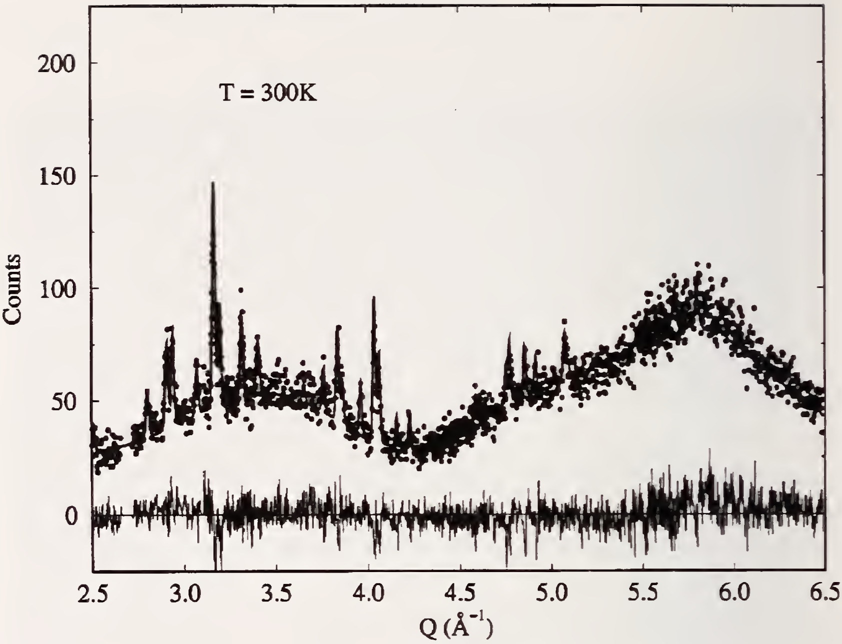

Fig. 21. The room temperature powder neutron diffraction pattern for C_{60}. Points represent the measurements and the solid line represents a calculation assuming that molecules are located on a face-centered cubic lattice, randomly oriented. A difference plot is included near the bottom of the figure.

III.4. Carbon-60

Buckminsterfullerene, C_{60}, was discovered in 1985, and a method of making macroscopic samples was reported about five years later. Since that time there has been considerable research activity in many different fields. One of the more fundamental problems has been to understand the structure of solid C_{60}, and some of the most useful information has come from diffraction experiments using neutrons (Copley et al., 1992). One of the reasons that neutrons have been so useful in structure studies of C_{60} has to do with the very high symmetry of the molecule. The scattering due to an icosahedral C_{60} molecule appears at relatively high Q, which is where the atomic scattering factor for x-rays, f(Q), is small so that signal-to-background becomes problematic in x-ray experiments.

Solid C_{60} is crystalline, with icosahedral molecules located at face-centered cubic lattice sites. The nearest neighbor distance between molecular centers is approximately 10 Å. The room temperature diffraction pattern, shown in

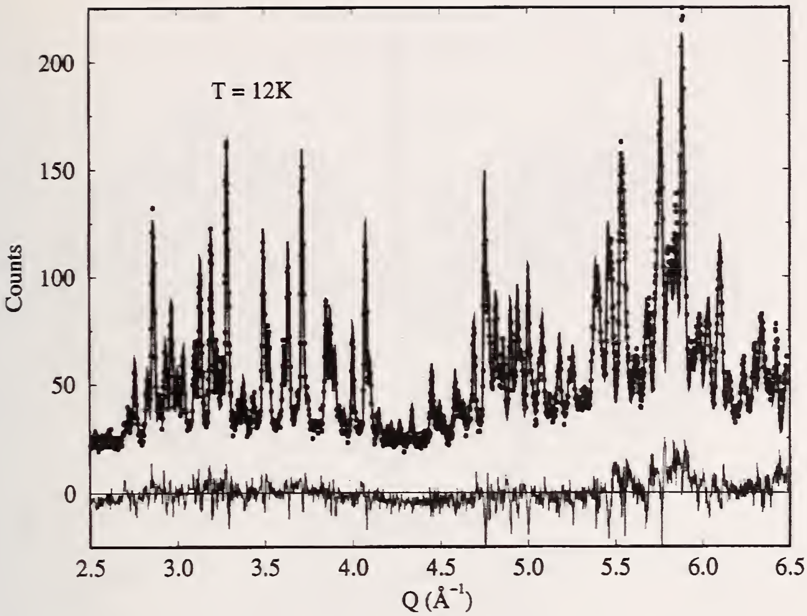

Fig. 22. The low temperature powder neutron diffraction pattern for C_{60}. Points represent the measurements and the solid line represents a calculation which assumes that each molecule adopts one of two possible orientations, pentagon-facing with probability 0.83 and hexagon-facing with probability 0.17, such that there are four molecules in the simple cubic unit cell. A difference plot is included near the bottom of the figure.

fig. 21, only has peaks at positions where peaks are predicted on the assumption that all molecules are structurally equivalent. On the other hand the low temperature diffraction pattern, shown in fig. 22, has additional peaks that imply that the molecules have become structurally inequivalent. A reasonable first approximation to the crystal structure of C_{60} is that below the first order orientational order-disorder transition temperature, $T_1 \approx 260$ K, each molecule adopts one of four possible orientations such that the unit cell is a simple cube containing four molecules (fig. 23), whereas above T_1 the molecules are randomly oriented.

The reader will have noticed that the relatively smooth "background" under the room temperature diffraction pattern (fig. 21) is intense, and curiously structured. It is in fact diffuse scattering which can be rather well explained as a consequence of the orientational disorder that is postulated to explain the Bragg peaks. Indeed the complete diffraction pattern (Bragg peaks plus diffuse scattering) can be described by a very simple model which assumes that all molecular orientations are equally likely. This picture of room temperature

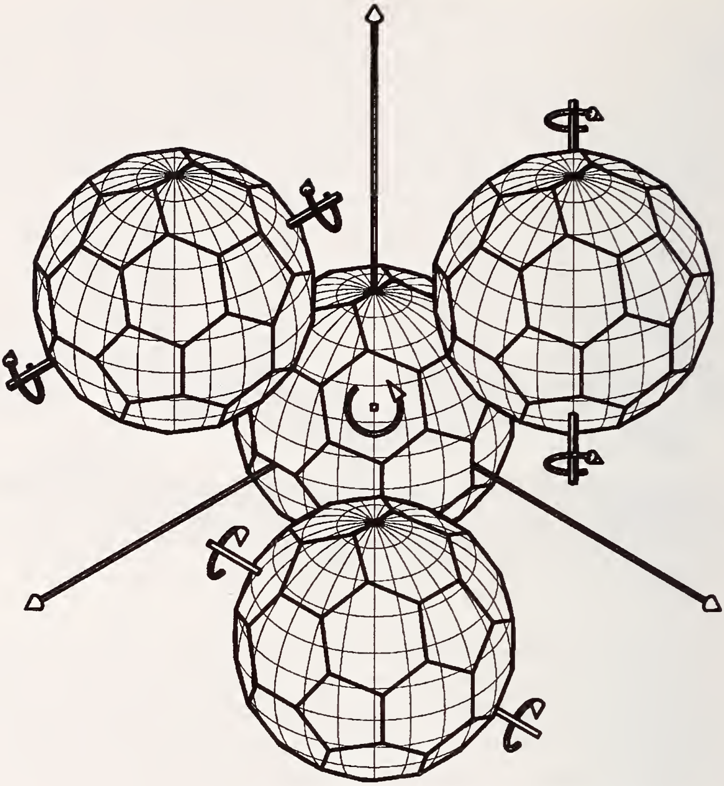

Fig. 23. A guide to understanding the crystal structure of C_{60}. Each ball represents a C_{60} molecule, with carbon atoms at each vertex connecting a pentagon and two hexagons. At all temperatures the centers of the molecules are located at face-centered cubic lattice sites. Above the phase transition the molecules are almost randomly oriented. Below the phase transition there are four molecules in the unit cell and each molecule in the unit cell has a different orientation. Each type of orientation, be it pentagon-facing or hexagon-facing, is obtained by rotating the molecules from their "standard" orientations (with 2-fold axes pointing along cube edge directions, as shown in the figure) through the same angle but about different (111) axes, as shown. For the pentagon-facing orientation the angle is about 98°; for the hexagon-facing orientation it is ≈38°.

C_{60} is certainly oversimplified, since the icosahedral symmetry of the C_{60} molecule and the cubic symmetry of the lattice must at some level influence the distribution of molecular orientations. To gain a better understanding of what is going on requires a multi-pronged approach, involving theory (e.g., Michel and Copley, 1997), computer simulations and experiments. Both neutrons and x-rays have been used, and there have been studies of powder samples and single crystals. The goal is to develop an improved representation of the interactions between the molecules in this fascinating material.

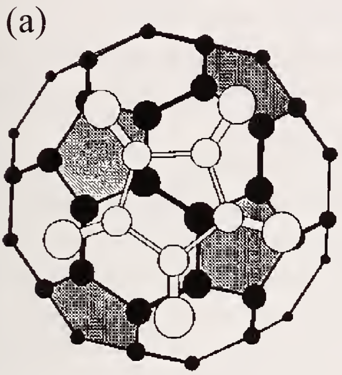

Fig. 24. Relative orientations of nearest neighbor molecules in the low temperature phase of C_{60}. Part of a neighboring molecule is viewed from within the molecule at the origin. The pentagon-facing orientation is shown at (a) and the hexagon-facing orientation is shown at (b). In each case the polygon (pentagon or hexagon) faces a hexagon-sharing "double bond" on the neighboring molecule.

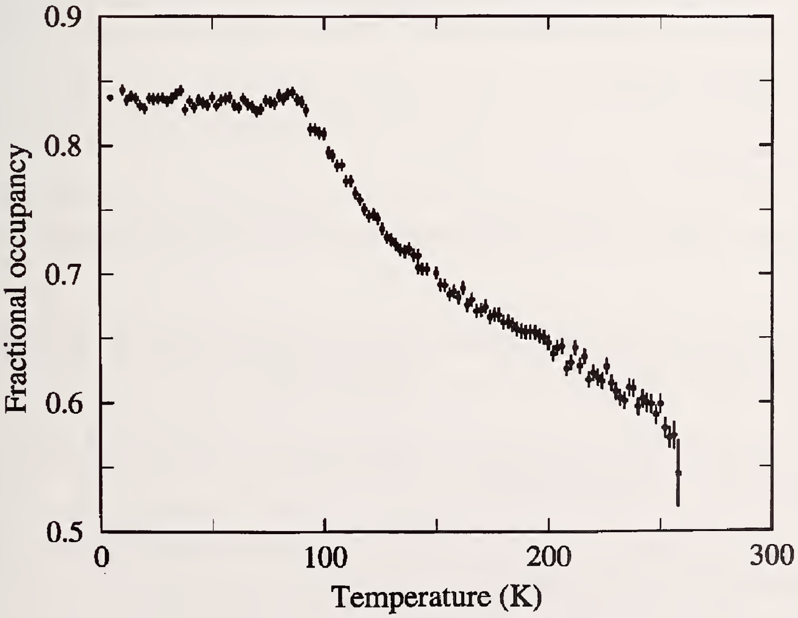

Fig. 25. The temperature dependence of the probability of the pentagon-facing orientation in low temperature C_{60}, as derived from neutron diffraction experiments (David et al., 1992).

Our description of the low temperature structure is also woefully incomplete. Powder neutron diffraction data (David et al., 1992) have shown that each molecule adopts two types of orientations (fig. 24), described as "pentagon-facing" and "hexagon-facing," and that the probability p that a molecule adopts the pentagon-facing orientation increases with decreasing temperature, as shown in fig. 25. Below ≈ 86K, p no longer changes with temperature, indicating that the system has frozen into an orientational glass.

The work described in the previous paragraph was performed using a time-of-flight diffractometer at a pulsed neutron source. Such instruments are well suited to measurements at large Q. A good example is a study of the structure of the C_{60} molecule itself, using data obtained up to Q-values as high as 50 $Å^{-1}$ (Soper et al., 1992). The extended range of Q was needed in order to be able to convert the data to a real space pair correlation function.

Acknowledgments

It is a pleasure to thank my colleagues at NIST, especially Julie Borchers, Paul Brand, Jeremy Cook, Qing-Zhen Huang, Jeff Lynn, David Mildner, Dan Neumann, Hank Prask, Louis Santodonato, Tony Santoro, Judith Stalick and Brian Toby, for helpful discussions, for the use of figures, and for the use of unpublished results.

References

G.E. Bacon (1975), "Neutron Diffraction," 3rd Ed. (Oxford University Press, Oxford).

P.C. Brand, H.J. Prask and G.E. Hicho (1996), National Institute of Standards and Technology Interagency Report NISTIR-5912.

J.R.D. Copley, D.A. Neumann, R.L. Cappelletti and W.A. Kamitakahara (1992), J. Phys. Chem. Solids **53**, 1353.

W.I.F. David, R.M. Ibberson, T.J.S. Dennis, J.P. Hare and K. Prassides (1992), Europhys. Lett. **18**, 219 and 735.

A. Fersht (1999), "Structure and Mechanism in Protein Science : A Guide to Enzyme Catalysis and Protein Folding" (W. H. Freeman, New York).

R.P. Feynman, R.B. Leighton and M. Sands (1963), "The Feynman Lectures on Physics," vol. 1, pp. 3-9 (Addison-Wesley, Reading, MA).

A. Furrer (1995) (ed.), "Magnetic Neutron Scattering" (World Scientific, Singapore).

A. Guinier (1963), "X-ray Diffraction in Crystals, Imperfect Crystals, and Amorphous Bodies" (W.H. Freeman, San Francisco and London).

Q. Huang, J.W. Lynn, Q. Xiong and C.W. Chu (1995), Phys. Rev. B**52**, 462.

Q. Huang, A. Santoro, J.W. Lynn, R.W. Erwin, J.A. Borchers, J.L. Peng, K. Ghosh and R.L. Greene (1998), Phys. Rev. B**58**, 2684.

Yu.A. Izyumov and R.P. Ozerov (1970), "Magnetic Neutron Diffraction" (Plenum, New York).

S.W. Lovesey (1987), "Theory of Neutron Scattering from Condensed Matter" (Oxford University Press, Oxford).

K.H. Michel and J.R.D. Copley (1997), Z. Phys. B**103**, 369.

H.J. Prask and P.C. Brand (1997), in "Neutrons in Research and Industry," ed. G. Vourvopoulos, SPIE Proceedings Vol. 2867, p. 106.

H.J. Prask and C.S. Choi (1993), in "Concise Encyclopaedia of Materials Characterization," eds. R.W. Cahn and E. Lifshin (Pergamon Press, Oxford), p. 497.

A.K. Soper, W.I.F. David, D.S. Sivia, T.J.S. Dennis, J.P. Hare and K. Prassides (1992), J. Phys.: Condens. Matter **4**, 6087.

G.L. Squires (1978), "Introduction to the Theory of Thermal Neutron Scattering" (Cambridge University Press, Cambridge), reprinted by Dover Publications, Mineola, NY (1996).

B.N. Taylor (1995), "Guide for the Use of the International System of Units (SI)," NIST Special Publication 811.

B.E. Warren (1969), "X-Ray Diffraction" (Addison-Wesley, Reading, MA), reprinted by Dover Publications, Mineola, NY (1990).

B.T.M. Willis and A.W. Pryor (1975), "Thermal Vibrations in Crystallography" (Cambridge University Press, Cambridge).

C.G. Windsor (1981), "Pulsed Neutron Scattering" (Taylor and Francis, London).

Q. Xiong, Y.Y. Xue, Y. Cao, F. Chen, Y.Y. Sun, J. Gibson, C.W. Chu, L.M. Liu and A. Jacobson (1994), Phys. Rev. B**50**, 10346.

R.A. Young (1993) (ed.), "The Rietveld Method" (Oxford University Press, Oxford).

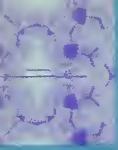

NIST CENTENNIAL 1901-2001

November 2001